Possible Fano Effect and Suppression of Andreev Reflection in $La_3Ni_2O_7$

Yi-feng Yang(杨义峰)[1,2,3*]

[1]*Beijing National Laboratory for Condensed Matter Physics and Institute of Physics, Chinese Academy of Sciences, Beijing 100190, China*
[2]*University of Chinese Academy of Sciences, Beijing 100049, China*
[3]*Songshan Lake Materials Laboratory, Guangdong 523808, China*

(Received 21 October 2024; accepted manuscript online 29 November 2024)

The recently discovered high-temperature superconductor $La_3Ni_2O_7$ under high pressure has sparked considerable debate. Central controversies revolve around whether interlayer or intralayer pairing mechanisms dominate and whether hybridization plays a crucial role in establishing superconductivity. However, experimental clarification remains challenging due to the limitations of state-of-the-art techniques under high-pressure conditions. Here, we propose that quasiparticle tunneling and Andreev reflection could offer practical methods to differentiate pairing scenarios. Specifically, we predict that hybridization between the $d_{x^2-y^2}$ metallic bands and the strongly renormalized flat d_{z^2} quasiparticle bands may induce an asymmetric Fano line shape. In the superconducting state, we show that Andreev reflection would be significantly suppressed in interlayer pairing superconductivity with limited interlayer hopping. We recommend future experiments to test these predictions and shed light on the fundamental physics of superconducting $La_3Ni_2O_7$ and other multi-layer nickelate superconductors.

DOI: 10.1088/0256-307X/42/1/017301 CSTR: 32039.14.0256-307X.42.1.017301

The discovery of high-temperature superconductivity in the bilayer nickelate $La_3Ni_2O_7$ under high pressure has triggered intense theoretical discussions about its electronic band structure and potential pairing mechanisms.[1–3] While ambient pressure experiments have resolved some key questions,[4–14] direct investigations of superconducting properties remain difficult due to the extreme pressures involved. A primary focus is understanding the nature of pairing mechanisms. Proposed interlayer pairings are often associated with interlayer superexchange interactions mediated by d_{z^2} orbitals.[15–31] However, some argue that the superconductivity resembles that of cuprates.[32–34] Debates also center on the role of Hund's rule coupling and the hybridization between $d_{x^2-y^2}$ and d_{z^2} orbitals.[17,25,27,35] In one model, hybridization facilitates long-range phase coherence by mobilizing local d_{z^2} interlayer pairs.[15,17] Conversely, in a Hund's coupling-based scenario, hybridization and d_{z^2} self-doping are detrimental. Here, Hund's rule coupling redirects interlayer superexchange from localized d_{z^2} orbitals to itinerant $d_{x^2-y^2}$ orbitals, forming interlayer Cooper pairs.[25] Distinguishing intralayer from interlayer pairing mechanisms and providing experimental evidence for hybridization is therefore essential.

However, high pressures have prevented the application of several important techniques. Among the very few exceptions, quasiparticle tunneling and Andreev reflection may be feasible methods to provide useful microscopic information on electronic and superconducting properties. In this study, we argue that they may exhibit distinct properties and help to distinguish different pairing scenarios in superconducting $La_3Ni_2O_7$. In particular, we show the possibility of a Fano effect in the quasiparticle tunneling spectra if hybridization indeed exists between the broad $d_{x^2-y^2}$ metallic bands and the strongly renormalized flat d_{z^2} quasiparticle bands, and that, in contrast to intralayer pairing superconductivity, the Andreev reflection may be greatly suppressed for interlayer pairing with small interlayer hopping. Future experiments should be conducted to verify these predictions.

We start with the following Hamiltonian with three parts:

$$H = H_{\rm s} + H_{\rm m} + H_{\rm c}, \tag{1}$$

where $H_{\rm s}$, $H_{\rm m}$, and $H_{\rm c}$ denote the nickelate superconductor, the normal metal lead, and their coupling terms, respectively. The $La_3Ni_2O_7$ Hamiltonian has an effective two-orbital bilayer form:[15,17,31]

$$\begin{aligned} H_{\rm s} = &\sum_{la\boldsymbol{k}s} \epsilon^a_{\boldsymbol{k}} d^\dagger_{la\boldsymbol{k}s} d_{la\boldsymbol{k}s} - \sum_{l\boldsymbol{k}s} V_{\boldsymbol{k}} (d^\dagger_{l1\boldsymbol{k}s} d_{l2\boldsymbol{k}s} + \text{h.c.}) \\ &- t_\perp \sum_{\boldsymbol{k}s} (d^\dagger_{11\boldsymbol{k}s} d_{21\boldsymbol{k}s} + \text{h.c.}) + J \sum_i \boldsymbol{S}_{1i} \cdot \boldsymbol{S}_{2i}, \end{aligned} \tag{2}$$

where $d^\dagger_{la\boldsymbol{k}\sigma}$ creates one d_{z^2} ($a = 1$) or $d_{x^2-y^2}$ ($a = 2$) electron of spin s and momentum $\boldsymbol{k}$ on l-th layer ($l = 1, 2$) $\boldsymbol{S}_{li} = \frac{1}{2}\sum_{ss'} d^\dagger_{l1is} \boldsymbol{\sigma}_{ss'} d_{l1is'}$ is the d_{z^2} spin density operator on site i of l-th layer with $\boldsymbol{\sigma}$ being the Pauli matrices, $\epsilon^a_{\boldsymbol{k}}$ gives the dispersion of a-th orbital within each layer, $V_{\boldsymbol{k}}$ is the intralayer nearest-neighbor hybridization between two orbitals, $t_\perp$ is the interlayer hopping of d_{z^2} quasiparticles,

*Corresponding author. Email: yifeng@iphy.ac.cn
© 2025 Chinese Physical Society and IOP Publishing Ltd. All rights, including for text and data mining, AI training, and similar technologies, are reserved.

and J is their interlayer superexchange interaction mediated by the apical oxygens.

The above effective t-V-J model is similar to the effective t-J model for cuprate superconductors and may be derived by projecting the double occupancy of the d_{z^2} orbitals from the bilayer two-orbital Hubbard model. As in cuprates, the degrees of freedom of oxygen are integrated. Whether a more complicated model containing all orbitals is necessary under certain circumstances requires further experimental scrutiny. First-principles calculations give $\epsilon^a_{\boldsymbol{k}} = -2t_a(\cos \boldsymbol{k}_x + \cos \boldsymbol{k}_y) + 4t'_a \cos \boldsymbol{k}_x \cos \boldsymbol{k}_y + \epsilon^a_0$ and $V_{\boldsymbol{k}} = -2V(\cos \boldsymbol{k}_x - \cos \boldsymbol{k}_y)$, where $t_1 = 0.11$, $t'_1 = -0.017$, $\epsilon^1_0 = 0.409$, $t_2 = 0.483$, $t'_2 = 0.069$, $\epsilon^2_0 = 0.776$, $V = 0.239$, and $t_\perp = 0.635$.[36] For simplicity, we omitted the energy unit eV throughout this study, unless noted otherwise. Other small parameters are ignored for simplicity, and their effects may be partially included by renormalizing the above tight-binding parameters.[17,37] The intralayer superexchange interaction is also ignored to focus only on the interlayer pairing because it is ten times smaller than the interlayer superexchange J as estimated recently from resonant inelastic X-ray scattering (RIXS) and inelastic neutron scattering (INS) measurements.[9,10] The lead and its coupling terms can be described as follows:

$$H_{\rm m} = \sum_{\boldsymbol{k}s} \xi_{\boldsymbol{k}} c^\dagger_{\boldsymbol{k}s} c_{\boldsymbol{k}s}, \quad H_{\rm c} = \sum_{a\boldsymbol{k}ps} t^a_{\boldsymbol{k}p} c^\dagger_{\boldsymbol{k}s} d_{1a\boldsymbol{p}s}, \tag{3}$$

where $\xi_{\boldsymbol{k}}$ is the dispersion of the noninteracting electrons in the normal metal lead, and $t^a_{\boldsymbol{k}}$ is the tunneling matrix in the a-th orbital. For simplicity, we explicitly consider only momenta $\boldsymbol{k}$ on the plane.

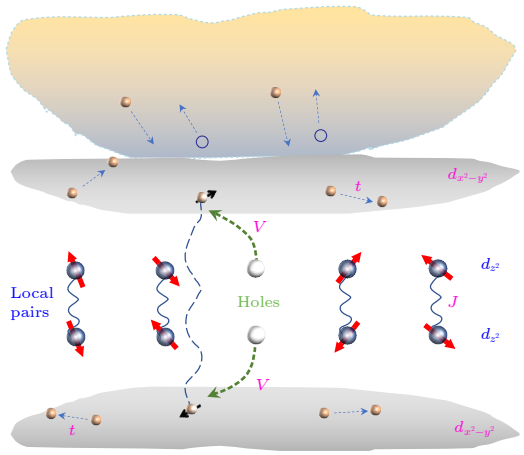

Fig. 1. Illustration of the normal metal/interlayer pairing superconductor junction and the effective t-V-J model for the bilayer nickelate, where t is the hopping parameter of the metallic band, J is the interlayer superexchange interaction of the local pairing orbital, and V is their hybridization. The electrons may tunnel into both the broad $d_{x^2-y^2}$ bands and the relatively narrow d_{z^2} bands in the top layer. The Fano interference arises because of the hybridization of the two bands. The Andreev reflection may be reduced when $t_\perp \to 0$ because of the interlayer pairing mechanism.

Figure 1 shows the schematic of this setup. Quasiparticle tunneling and Andreev reflection can be studied using the Keldysh Green's function technique.[38] Applying a bias voltage $V_{\rm b}$ to the lead induced a finite electric current,[39–41]

$$\begin{aligned} I &= -e\frac{dN_c}{dt} = -i\frac{e}{\hbar}\sum_{a\boldsymbol{k}qs} t^a_{\boldsymbol{k}q}\langle d^\dagger_{1a\boldsymbol{q}s} c_{\boldsymbol{k}s}\rangle + \text{c.c.} \\ &= \frac{e}{h}\int d\omega [f(\omega - eV_{\rm b}) - f(\omega)]T(\omega), \end{aligned} \tag{4}$$

where $N_c = \sum_{\boldsymbol{k}s} c^\dagger_{\boldsymbol{k}s} c_{\boldsymbol{k}s}$ is the total number of electrons in the lead, $f(\omega)$ is the Fermi distribution function, and the scattering matrix is given by

$$T(\omega) = \sum_{aa'a''\boldsymbol{k}pqs} \Gamma^0_{\boldsymbol{k}} \Gamma^{aa'}_{\boldsymbol{q}p} \mathcal{G}^{\rm R}_{a'\boldsymbol{p}s,a''\boldsymbol{k}s}(\omega) \mathcal{G}^{\rm A}_{a''\boldsymbol{k}s,a\boldsymbol{q}s}(\omega), \tag{5}$$

where $\Gamma^0_{\boldsymbol{k}}$ measures the quasiparticle line width in the top NiO layer, $\Gamma^{aa'}_{\boldsymbol{q}p} = 2\pi \sum_{\boldsymbol{k}'} t^a_{\boldsymbol{k}'q} t^{a'}_{\boldsymbol{p}\boldsymbol{k}'} \rho^c_{\boldsymbol{k}'s}(\omega)$ with $\rho^c_{\boldsymbol{k}'s}(\omega)$ being the spectral function of the lead electrons, and $\mathcal{G}^{\rm R/A}$ denote the retarded/advanced Green's functions of the top layer ($l = 1$) in the Nambu representation $\psi^\dagger_{\boldsymbol{k}} = (d^\dagger_{11\boldsymbol{k}\uparrow}, d^\dagger_{12\boldsymbol{k}\uparrow}, d_{11\bar{\boldsymbol{k}}\downarrow}, d_{12\bar{\boldsymbol{k}}\downarrow})$. Thus, the total scattering can be split into two terms: $T(\omega) = T^{\rm Q}(\omega) + T^{\rm A}(\omega)$, where $T^{\rm Q}$ and $T^{\rm A}$ describe the quasiparticle tunneling and Andreev reflection contributions, respectively. We have

$$\begin{aligned} T^{\rm Q}(\omega) &= \sum_{aa'a''\boldsymbol{k}pqs} \Gamma^0_{\boldsymbol{k}} \Gamma^{aa'}_{\boldsymbol{q}p} G^{\rm R}_{a'\boldsymbol{p}s,a''\boldsymbol{k}s}(\omega) G^{\rm A}_{a''\boldsymbol{k}s,a\boldsymbol{q}s}(\omega), \\ T^{\rm A}(\omega) &= \sum_{aa'a''\boldsymbol{k}pqs} \Gamma^0_{\bar{\boldsymbol{k}}} \Gamma^{aa'}_{\boldsymbol{q}p} F^{\rm R}_{a'\boldsymbol{p}s,a''\bar{\boldsymbol{k}}\bar{s}}(\omega) F^{\dagger,A}_{a''\bar{\boldsymbol{k}}\bar{s},a\boldsymbol{q}s}(\omega), \end{aligned} \tag{6}$$

where $G^{\rm R/A}$ and $F^{\rm R/A}$ are the normal and anomalous components of the Green's function $\mathrm{G}^{\rm R/A}$ in the Nambu representation, respectively. In the following sections, we discuss $T^{\rm Q}$ and $T^{\rm A}$ separately.

In the formalism above, only Green's functions of the top layer ($l = 1$) are explicitly involved. To calculate them, we employ the mean-field approximation and decouple the superexchange term, $J\boldsymbol{S}_{1i} \cdot \boldsymbol{S}_{2i} \to \sqrt{2}(\Delta^* \Phi_i + \bar{\Phi}_i \Delta)$, where $\Phi_i = \frac{1}{\sqrt{2}}(d_{11i\downarrow} d_{21i\uparrow} - d_{11i\uparrow} d_{21i\downarrow})$ represents the local interlayer d_{z^2} pairing at site i and Δ is the corresponding static uniform pairing field. Note that the interlayer pairing of $d_{x^2-y^2}$ electrons was induced through hybridization, as discussed in Refs. [15,17]. The mean-field approximation ignores the correlation effects as well as the spatial and temporal fluctuations of superconductivity; thus, all energy scales may be strongly renormalized and altered in real experiments, particularly near the Fermi energy. Nevertheless, it provides a reasonable starting point for studying the qualitative features of quasiparticle tunneling and Andreev reflections. Under the mean-field approximation, the Hamiltonian takes a bilinear form, which can be solved straightforwardly in momentum space. However, coupling to the lead may introduce momentum scattering and complicate calculations. To simplify the calculations, we ignore the off-diagonal contribution in $\mathcal{T}^{\rm Q/A}$ by replacing $G_{\boldsymbol{p}k} \to G_{\boldsymbol{k}} \delta_{\boldsymbol{p}k}$ and $F_{\boldsymbol{p}\bar{k}} \to F_{\boldsymbol{k}} \delta_{\boldsymbol{p}k}$ or equivalently $\Gamma^{aa'}_{\boldsymbol{q}p} \to \Gamma^{aa'}_{\boldsymbol{k}} \delta_{\boldsymbol{p}k} \delta_{\boldsymbol{q}k}$ in Eq. (6). This may have some

quantitative influence but does not affect our major conclusions, which depend only on the presence or absence of hybridization and interlayer coupling.

The Green's functions for the top layer were obtained by integrating the electron degrees of freedom of the lead and bottom layers ($l = 2$). Under the Nambu basis, $\psi_{\boldsymbol{k}}$, we derive the following matrix form:

$$(\mathcal{G}^{\rm R}_{\boldsymbol{k}})^{-1} = g^{-1}_{\boldsymbol{k}} I - \mathcal{H}^0_{\boldsymbol{k}} - \Sigma_{\boldsymbol{k}} - M[g^{-1}_{\boldsymbol{k}} I - \mathcal{H}^0_{\boldsymbol{k}}]^{-1} M^{\dagger}, \quad (7)$$

where $g^{-1}_{\boldsymbol{k}} = \omega + i\Gamma^0_{\boldsymbol{k}}/2$, I is a 4×4 unit matrix, and

$$\mathcal{H}^0_{\boldsymbol{k}} = \begin{pmatrix} \epsilon^1_{\boldsymbol{k}} & -V_{\boldsymbol{k}} & 0 & 0 \\ -V_{\boldsymbol{k}} & \epsilon^2_{\boldsymbol{k}} & 0 & 0 \\ 0 & 0 & -\epsilon^1_{\tilde{\boldsymbol{k}}} & V_{\tilde{\boldsymbol{k}}} \\ 0 & 0 & V_{\tilde{\boldsymbol{k}}} & -\epsilon^2_{\tilde{\boldsymbol{k}}} \end{pmatrix},$$

$$M = \begin{pmatrix} -t_\perp & 0 & \Delta & 0 \\ 0 & 0 & 0 & 0 \\ \Delta^* & 0 & t_\perp & 0 \\ 0 & 0 & 0 & 0 \end{pmatrix},$$

$$\Sigma_{\boldsymbol{k}} = -\frac{i}{2}\begin{pmatrix} \Gamma^{11}_{\boldsymbol{k}} & \Gamma^{12}_{\boldsymbol{k}} & 0 & 0 \\ \Gamma^{21}_{\boldsymbol{k}} & \Gamma^{22}_{\boldsymbol{k}} & 0 & 0 \\ 0 & 0 & \Gamma^{11}_{\tilde{\boldsymbol{k}}} & \Gamma^{12}_{\tilde{\boldsymbol{k}}} \\ 0 & 0 & \Gamma^{21}_{\tilde{\boldsymbol{k}}} & \Gamma^{22}_{\tilde{\boldsymbol{k}}} \end{pmatrix}. \quad (8)$$

For simplicity, we further ignore the momentum dependence in $\Gamma^0_{\boldsymbol{k}}$ and $\Gamma^{11}_{\boldsymbol{k}}$, assume $\Gamma^0_{\boldsymbol{k}} \equiv \Gamma^0$, $\Gamma^{11}_{\boldsymbol{k}} \equiv \Gamma^{11}$, $\Gamma^{12/21}_{\boldsymbol{k}} = \Gamma^{12/21}(\cos\boldsymbol{k}_x - \cos\boldsymbol{k}_y)$, and $\Gamma^{22}_{\boldsymbol{k}} = \Gamma^{22}(\cos\boldsymbol{k}_x - \cos\boldsymbol{k}_y)^2$, and set $\Gamma^{12} = \Gamma^{21} = r\Gamma^{22}$ and $\Gamma^{11} = r^2\Gamma^{22}$. Here r is the ratio of the tunneling t^a into d_{z^2} and $d_{x^2-y^2}$ orbitals and $(\cos\boldsymbol{k}_x - \cos\boldsymbol{k}_y)$ accounts for the effect of the sign change of the $d_{x^2-y^2}$ wave function along x and y directions on $t^2_{\boldsymbol{k}}$ assuming the lead electrons have isotropic wave functions. We also require Δ, Γ^0, Γ^{22}, and r to be real numbers.

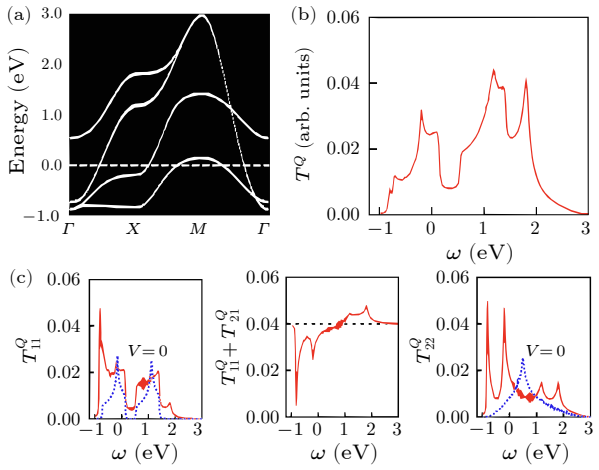

Fig. 2. (a) Spectral function calculated based on the tight-binding parameters and $\Gamma^0 = \Gamma^{aa'} = 0.01$. (b) The corresponding quasiparticle tunneling spectra showing multiple peaks. (c) Three components of the quasiparticle tunneling coefficient, showing a significant contribution from the off-diagonal term. The dotted lines show $T^{\rm Q}_{11}$ and $T^{\rm Q}_{22}$ at $V = 0$ for comparison.

To verify the formalism above, we first show in Fig. 2(a) the calculated spectral function $A_{\boldsymbol{k}}(\omega) = -\pi^{-1}{\rm Im}\sum_{as} G^{\rm R}_{1a\boldsymbol{k}s,\,1a\boldsymbol{k}s}(\omega)$ along a high symmetry path for $\Gamma^0 = \Gamma^{22} = 0.01$, $r = 1$, and $\Delta = 0$ using the tight-binding parameters. Direct comparisons with previous works confirm the derived band structures, which contain both bonding (around the Fermi energy) and antibonding bands of d_{z^2} orbitals and several flat pieces induced by their hybridization with the broader $d_{x^2-y^2}$ bands.[36] By substituting the derived Green functions into Eq. (6) yields the quasiparticle tunneling coefficient $T^{\rm Q}(\omega)$. The numerical results are presented in Fig. 2(b) and exhibit multiple pronounced peaks corresponding to the flat pieces of the bands, which reflect the interplay between the van Hove singularities and the hybridization between the d_{z^2} and $d_{x^2-y^2}$ bands. For clarity, Fig. 2(c) presents its three components, $T^{\rm Q}_{11}$, $T^{\rm Q}_{12}+T^{\rm Q}_{21}$, and $T^{\rm Q}_{22}$, where $T^{\rm Q}_{aa'} = \sum_{a''\boldsymbol{k}s}\Gamma^0_{\boldsymbol{k}}\Gamma^{aa'}_{\boldsymbol{k}}G^{\rm R}_{1a'\boldsymbol{k}s,\,1a''\boldsymbol{k}s}G^{\rm A}_{1a''\boldsymbol{k}s,\,1a\boldsymbol{k}s}$. There is a substantial contribution from the interference term $\mathcal{T}^{\rm Q}_{12} + \mathcal{T}^{\rm Q}_{21}$, particularly at negative energies, where a sharp peak is almost completely cancelled out by those in $T^{\rm Q}_{11}$ and $T^{\rm Q}_{22}$. This corresponds to a flat band close to -1, which will be renormalized towards the Fermi energy once the correlation effects are correctly considered. The valley between 0 and 0.5 only appears in $T^{\rm Q}_{11}$, corresponding to the bonding-antibonding splitting region of the d_{z^2} bands, below which the low-energy physics are governed by the bonding orbitals. For comparison, the quasiparticle tunneling coefficients without hybridization ($V = 0$) are shown in Fig. 2(c).

To obtain a better view of the interference effect in the low-energy region, Fig. 3 plots the quasiparticle tunneling coefficient in a smaller energy window around the Fermi energy and consider the renormalization effect by tuning $\epsilon^1_{\boldsymbol{k}} \to \eta_t\epsilon^1_{\boldsymbol{k}}$, $t_\perp \to \eta_t t_\perp$, and $V \to \eta_V V$, where η_t and η_V arises from the Gutzwiller projection for the nearly half-filled d_{z^2} orbitals in $La_3Ni_2O_7$ but are taken here as free parameters. Figure 3(a) shows the temperature evolution of differential conductance $G(V_{\rm b}) = dI(V_{\rm b})/dV_{\rm b}$ as a function of the bias voltage for $\eta_t = 0$, $\eta_V = 0.5$, $\Gamma^0 = \Gamma^{22} = 0.01$, and $r = 0.2$. We deliberately chose the extreme case with $\eta_t = 0$ to reflect strongly renormalized flat d_{z^2} quasiparticle bands to be able to ignore other complications, as shown in Fig. 2, and focus only on the hybridization effect in the quasiparticle tunneling. The ratio r of the tunneling parameters into d_{z^2} and $d_{x^2-y^2}$ orbitals should be correspondingly renormalized and assigned a small number, which suppresses the d_{z^2} quasiparticle weight ignored in the mean-field approximation. In an extreme case where d_{z^2} electrons are fully localized, possibly at ambient pressure, we should have $\eta_t = \eta_V = r = 0$ and the electrons can only tunnel into the $d_{x^2-y^2}$ orbital, producing a broad background.

As illustrated in Fig. 3(a), the differential conductance $G(V_{\rm b})$ exhibits an asymmetric feature below the Fermi energy, approximately following a Fano-like line shape superimposed on the broad background of the $d_{x^2-y^2}$ metallic bands without hybridization. The suppression observed

below $V = 0$ is attributed to destructive interference arising from the off-diagonal term $T^{\rm Q}_{12}+T^{\rm Q}_{21}$, absent in the case of no hybridization. This is further clarified in Fig. 3(b), which decomposes the quasiparticle tunneling coefficient $T^{\rm Q}(\omega)$ into its three components. Notably, the off-diagonal term remains nearly constant around $\omega = -0.2$, canceling out the diagonal contributions from $T^{\rm Q}_{11}(\omega)$ and $T^{\rm Q}_{22}(\omega)$ and producing a conductance minimum at a negative V slightly below zero bias. At low temperatures, this suppression in $G(V_{\rm b})$ is interrupted by an unexpected peak at $V = 0$. This peak, appearing exclusively in $T^{\rm Q}_{11}$ [Fig. 3(b)], is a property specific to d_{z^2} orbitals. We attribute it to nodal hybridization along the zone diagonal ($k_x = k_y$) direction, leaving a finite contribution from the d_{z^2} flat bands at the Fermi energy. Thus, the Fano interference effect results from hybridization between the strongly renormalized flat d_{z^2} quasiparticle bands and the broad metallic $d_{x^2-y^2}$ bands.

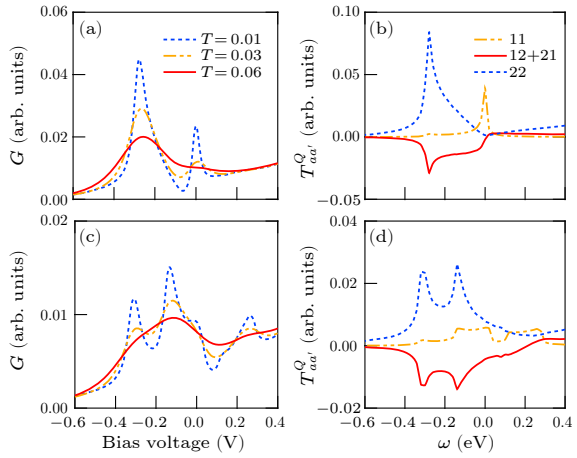

Fig. 3. (a) Differential conductance $G = dI(V_{\rm b})/dV_{\rm b}$ from quasiparticle tunneling for the tight-binding parameters with $\eta_t = 0$, $\eta_V = 0.5$, $\Gamma^0 = \Gamma^{22} = 0.01$, and $r = 0.2$ for the temperature $T = 0.01$, 0.03, and 0.06. (b) Three components of the corresponding quasiparticle tunneling coefficient, $T^{\rm Q}_{11}$, $T^{\rm Q}_{12}+T^{\rm Q}_{21}$, and $T^{\rm Q}_{22}$. (c) Differential conductance $G = dI/dV$ for the tight-binding parameters with $\eta_t = 0.2$, $\eta_V = 0.5$, $\Gamma^0 = \Gamma^{22} = 0.01$, and $r = 0.3$ for $T = 0.01$, 0.03, 0.06, showing additional peaks due to the bonding-antibonding splitting at low temperatures but a broad asymmetric line shape at high temperatures. (d) Three components of the quasiparticle tunneling coefficient, $T^{\rm Q}_{11}$, $T^{\rm Q}_{12}+T^{\rm Q}_{21}$, and $T^{\rm Q}_{22}$ for (c). For simplicity, we ignored the temperature dependence of all parameters.

However, due to the complexity of realistic electronic structures, the experimental observability of the Fano effect is uncertain. To explore this, Fig. 3(c) shows differential conductance for a finite $\eta_t = 0.2$, corresponding to narrow yet dispersive d_{z^2} quasiparticle bands. The other parameters remain largely unchanged, except for a slightly increased $r = 0.3$. At low temperatures, the $G(V_{\rm b})$ curve changes significantly, with the single peak near -0.3 V in Fig. 3(a) splitting into two, while the peak at the Fermi energy is suppressed. These changes arise from the finite dispersion and bonding-antibonding splitting of d_{z^2} quasiparticle bands for $\eta_t = 0.2$. Consequently, many additional peaks emerge, rendering the Fano feature indistinguishable. However, at a higher temperature ($T = 0.03$), peak broadening restores an overall asymmetric line shape on a broad background, indicating hybridization-induced interference. For completeness, Fig. 3(d) compares the three components of the corresponding tunneling coefficient. The off-diagonal contribution remains substantial and negative, reinforcing destructive interference. However, this term may be overshadowed if the lead's coupling to the d_{z^2} orbital is too strong (large r). This possibility arises because, despite its small spectral weight, the d_{z^2} quasiparticle wave function, oriented perpendicular to the NiO plane, may overlap more with the lead electrons than the $d_{x^2-y^2}$ orbital. Consequently, the zero-bias differential conductance is dominated by the d_{z^2} spectra, as reflected in $T^{\rm Q}_{11}(\omega)$. Future experiments are needed to confirm whether the hybridization-induced Fano interference effect can be observed in pressurized $La_3Ni_2O_7$. The outcome likely depends on the experimental parameter range. Similar Fano phenomena have been predicted and observed in heavy fermion systems. [42]

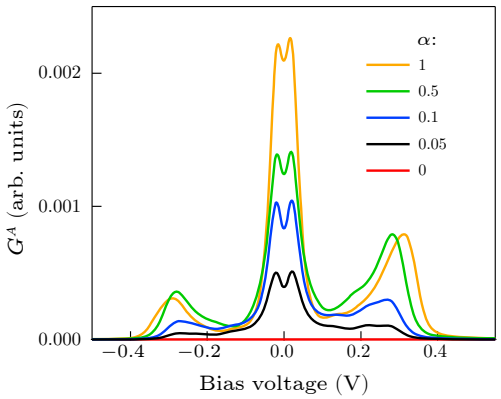

Fig. 4. (a) Different conductance contributed by the Andreev reflection coefficient using the tight-binding parameters with $\eta_t = 0.2$, $\eta_V = 0.5$, $\Gamma^0 = \Gamma^{22} = 0.01$, $r = 0.3$, and the pairing order parameter $\Delta = 0.02$ for the renormalized $t_\perp \to \alpha\eta_t t_\perp$ with varying $\alpha = 1$, 0.5, 0.1, 0.05, 0 at $T = 0.01$.

We now turn to the superconducting state and analyze the Andreev reflection for interlayer pairing. Figure 4 illustrates the differential conductance $G^{\rm A}(V_{\rm b})$, solely contributed by the Andreev reflection coefficient $T^{\rm A}(\omega)$, assuming $\Delta = 0.02$ for interlayer pairing. To examine the effect of interlayer hopping, we scale $\eta_t t_\perp \to \alpha\eta_t t_\perp$ by introducing an additional factor $\alpha = 0.5$, 0.1, 0.05, and 0. All other parameters match those in Fig. 3(d). For finite α, an Andreev reflection peak is clearly visible around zero bias, contrasting with the V- or U-shaped gap in the quasiparticle tunneling contribution. However, as α decreases, the peak height gradually diminishes and ultimately vanishes for $\alpha = 0$. This behavior indicates that Andreev reflection is entirely suppressed without interlayer hopping, a distinguishing feature of interlayer pairing superconductivity. This suppression is analogous to the junction behavior between a fully polarized ferromagnet and a

spin-singlet superconductor. The reasoning is straightforward: Andreev reflection occurs only if incident electrons form Cooper pairs in the superconductor and reflect as holes. For interlayer pairing superconductivity, this process is impossible if the electrons can only tunnel into the top layer when $t_\perp = 0$. A finite $t_\perp$ not only generates a higher-order intralayer pairing component but also facilitates tunneling into the bottom layer, thereby allowing a finite Andreev reflection coefficient. For small $t_\perp$, renormalized by strong electronic correlations and proportional to the self-doped hole density in nearly half-filled d_{z^2} orbitals, Andreev reflection is significantly weaker. This behavior, which should show systematic evolution with pressure or d_{z^2} hole doping, sharply contrasts with extensively studied intralayer pairing scenarios.[43] Nonetheless, care must be taken to exclude other factors, such as junction transparency, which can also suppress Andreev reflections.

It is important to note that we did not attempt quantitative predictions of experimental observations, as these are highly sensitive to setup specifics, including contact and surface quality, as well as compound parameters. Additionally, high-pressure measurements pose substantial challenges. The mean-field approximation cannot fully capture the strongly correlated nature of the system. Furthermore, determining the pairing symmetry will likely require extensive phase-sensitive experiments. Our focus was to highlight two general properties of interlayer pairing superconductivity in the t-V-J model: the potential occurrence of hybridization-induced Fano interference and the suppression of Andreev reflection in the absence of interlayer tunneling. These qualitative conclusions, independent of many details, may also apply to the trilayer $La_4Ni_3O_{10}$ system under similar conditions.[44] While material complexities may hinder experimental observations of these features, their identification could still provide valuable insights into the fundamental physics of nickelate high-temperature superconductors under pressure.

Acknowledgment. This work was supported by the National Natural Science Foundation of China (Grant No. 12474136), the Strategic Priority Research Program of the Chinese Academy of Sciences (Grant No. XDB33010100), and the National Key Research and Development Program of China (Grant No. 2022YFA1402203).

References

[1] Sun H, Huo M, Hu X, Li J, Liu Z, Han Y, Tang L, Mao Z, Yang P, Wang B, Cheng J, Yao D X, Zhang G M, and Wang M 2023 *Nature* **621** 493
[2] Hou J, Yang P T, Liu Z Y, Li J Y, Shan P F, Ma L, Wang G, Wang N N, Guo H Z, Sun J P, Uwatoko Y, Wang M, Zhang G M, Wang B S, and Cheng J G 2023 *Chin. Phys. Lett.* **40** 117302
[3] Zhang Y, Su D, Huang Y, Shan Z, Sun H, Huo M, Ye K, Zhang J, Yang Z, Xu Y, Su Y, Li R, Smidman M, Wang M, Jiao L, and Yuan H 2024 *Nat. Phys.* **20** 1269
[4] Yang J, Sun H, Hu X, Xie Y, Miao T, Luo H, Chen H, Liang B, Zhu W, Qu G, Chen C Q, Huo M, Huang Y, Zhang S, Zhang F, Yang F, Wang Z, Peng Q, Mao H, Liu G, Xu Z, Qian T, Yao D X, Wang M, Zhao L, and Zhou X J 2024 *Nat. Commun.* **15** 4373
[5] Liu Z, Huo M, Li J, Li Q, Liu Y, Dai Y, Zhou X, Hao J, Lu Y, Wang M, and Wen H H 2024 *Nat. Commun.* **15** 7570
[6] Chen K, Liu X, Jiao J, Zou M, Jiang C, Li X, Luo Y, Wu Q, Zhang N, Guo Y, and Shu L 2024 *Phys. Rev. Lett.* **132** 256503
[7] Dong Z, Huo M, Li J, Li J, Li P, Sun H, Lu Y, Wang M, Wang Y, and Chen Z 2024 *Nature* **630** 847
[8] Li Y, Du X, Cao Y, Pei C, Zhang M, Zhao W, Zhai K, Xu R, Liu Z, Li Z, Zhao J, Li G, Qi Y, Guo H, Chen Y, and Yang L 2024 *Chin. Phys. Lett.* **41** 087402
[9] Xie T, Huo M, Ni X, Shen F, Huang X, Sun H, Walker H C, Adroja D, Yu D, Shen B, He L, Cao K, and Wang M 2024 arXiv:2401.12635 [cond-mat.supr-con]
[10] Chen X, Choi J, Jiang Z, Mei J, Jiang K, Li J, Agrestini S, Garcia-Fernandez M, Huang X, Sun H, Shen D, Wang M, Hu J, Lu Y, Zhou K J, and Feng D 2024 *Nat. Commun.* **15** 9597
[11] Dan Z, Zhou Y, Huo M, Wang Y, Nie L, Wang M, Wu T, and Chen X 2024 arXiv:2402.03952 [cond-mat.supr-con]
[12] Abadi S N, Xu K, Lomeli E G, Puphal P, Isobe M, Zhong Y, Fedorov A V, Mo S, Hashimoto M, Lu D, Moritz B, Keimer B, Devereaux T P, Hepting M, and Shen Z X 2024 arXiv:2402.07143 [cond-mat.supr-con]
[13] Li Y D, Cao Y T, Liu L Y, Peng P, Lin H, Pei C Y, Zhang M X, Wu H, Du X, Zhao W X, Zhai K Y, Zhao J K, Lin M L, Tan P H, Qi Y P, Li G, Guo H J, Yang L, and Yang L X 2024 arXiv:2403.05012 [cond-mat.supr-con]
[14] Wang M, Wen H H, Wu T, Yao D X, and Xiang T 2024 *Chin. Phys. Lett.* **41** 077402
[15] Qin Q and Yang Y F 2023 *Phys. Rev. B* **108** L140504
[16] Yang Q G, Wang D, and Wang Q H 2023 *Phys. Rev. B* **108** L140505
[17] Yang Y F, Zhang G M, and Zhang F C 2023 *Phys. Rev. B* **108** L201108
[18] Liu Y B, Mei J W, Ye F, Chen W Q, and Yang F 2023 *Phys. Rev. Lett.* **131** 236002
[19] Shen Y, Qin M, and Zhang G M 2023 *Chin. Phys. Lett.* **40** 127401
[20] Gu Y, Le C, Yang Z, Wu X, and Hu J 2023 arXiv:2306.07275
[21] Zheng Y Y and Wú W 2023 arXiv:2312.03605
[22] Zhang Y, Lin L F, Moreo A, Maier T A, and Dagotto E 2024 *Nat. Commun.* **15** 2470
[23] Qu X Z, Qu D W, Chen J, Wu C, Yang F, Li W, and Su G 2024 *Phys. Rev. Lett.* **132** 036502
[24] Sakakibara H, Kitamine N, Ochi M, and Kuroki K 2024 *Phys. Rev. Lett.* **132** 106002
[25] Lu C, Pan Z, Yang F, and Wu C 2024 *Phys. Rev. Lett.* **132** 146002
[26] Heier G, Park K, and Savrasov S Y 2024 *Phys. Rev. B* **109** 104508
[27] Tian Y H, Chen Y, Wang J M, He R Q, and Lu Z Y 2024 *Phys. Rev. B* **109** 165154
[28] Chen J, Yang F, and Li W 2024 *Phys. Rev. B* **110** L041111
[29] Luo Z, Lv B, Wang M, Wú W, and Yao D X 2024 *npj Quantum Mater.* **9** 61
[30] Xue J R and Wang F 2024 *Chin. Phys. Lett.* **41** 057403
[31] Wang J and Yang Y F 2024 arXiv:2408.09774
[32] Fan Z, Zhang J F, Zhan B, Lv D, Jiang X Y, Normand B, and Xiang T 2024 *Phys. Rev. B* **110** 024514
[33] Jiang K, Wang Z Q, and Zhang F C 2024 *Chin. Phys. Lett.* **41** 017402
[34] Jiang R, Hou J, Fan Z, Lang Z J, and Ku W 2024 *Phys. Rev. Lett.* **132** 126503
[35] Qu X Z, Qu D W, Li W, and Su G 2023 arXiv:2311.12769
[36] Luo Z, Hu X, Wang M, Wú W, and Yao D X 2023 *Phys. Rev. Lett.* **131** 126001)

[37] Cao Y and Yang Y F 2024 *Phys. Rev. B* **109** L081105
[38] Haug H and Jauho A P 1998 *Quantum Kinetics in Transport and Optics of Semiconductors* (Springer-Verlag, Berlin)
[39] Meir Y and Wingreen N S 1992 *Phys. Rev. Lett.* **68** 2512
[40] Yang Y F and Lin T H 2001 *Phys. Rev. B* **64** 233314
[41] Dai Y X and Sun Q F 2024 *Phys. Rev. B* **109** 144504
[42] Yang Y F 2009 *Phys. Rev. B* **79** 241107
[43] Deutscher G 2005 *Rev. Mod. Phys.* **77** 109
[44] Qin Q, Wang J, and Yang Y F 2024 *The Innovation Materials* **2** 100102